NDT&E International 62 (2014) 1–5

Contents lists available at ScienceDirect

NDT&E International

journal homepage: www.elsevier.com/locate/ndteint

Micromagnetic technology for detection of carbon impurity in crystalline silicon

Runqiao Yu *[,1], Bo Hu [1], Hengcai Zou, Wenbo Xiao, Qiangqiang Cheng, Weijin Xu, Jijun Xin

Key Laboratory of Nondestructive Testing (Ministry of Education), Nanchang Hang Kong University, Nanchang 330063, PR China

ARTICLE INFO

Article history:
Received 17 April 2013
Received in revised form
9 October 2013
Accepted 11 October 2013
Available online 19 October 2013

Keywords:
Crystalline silicon
Carbon impurity
Micromagnetic detection
Magnetic susceptibility

ABSTRACT

This paper proposes a method of lossless micromagnetic detection in the geomagnetic field for detecting traces of carbon impurity defects in crystalline silicon. The magnetization tests show that crystalline silicon is a diamagnetic substance with a stronger relative permeability than carbon. Micromagnetic decay theory is gained according to the energy decay. When the geomagnetic field penetrates through the materials, the apparent magnetic susceptibility can be calculated and subsequently used to project the images. The resulting image clearly showed the location of the defects. Test results are proved by the metallographic phase and spectral analysis. New method and ideas are provided for effective detection of trace carbon impurity defects in the crystalline silicon.

1. Introduction

The most common raw material used in solar panels is crystalline silicon, which is approximately 99.9999% pure. No standard currently exists to test the performance of crystalline silicon, although the amount of internal and surface impurities present in the crystalline silicon body is a key parameter. Therefore, testing the content and distribution of major impurities in the crystalline silicon is vital for the development and utilization of solar energy. These defect detection methods of crystalline silicon fall into two categories based on defect type: crack detection and impurity detection. Belyaev [1] and Dallas [2] presented an experimental method of rapid crack detection and length determination in full-sized, solar-grade crystalline silicon wafers using the resonance ultrasonic vibrations technique. Hilmersson [3] performed an acoustic measurement by mechanically exciting the vibratory modes of single-crystalline silicon wafers with different hairline periphery cracks and at different locations. His results suggested that an impact test method may be useful for solar cell crack detection and quality control. Chakrapani [4] used the Lamb wave air-coupled ultrasonic testing to examine the cracks in full-sized Cz-silicon wafers. Chiou and Liu [5] applied machine vision techniques to micro-crack detection in multi-crystalline silicon solar wafers; the developed prototype system detected micro-cracks down to 13.4 mm.

The major impurity elements found in the crystalline silicon used in solar panels consist of nonmetallic impurities (such as boron, phosphorus, and carbon) and metallic impurities (including iron, aluminum, and copper). Specific detection methods can be found in [6]. Mass spectrometry [7–12] has attracted the attention of the crystalline silicon industry because of its element detection abilities, simple spectrum diagrams, high sensitivity, fast analysis, and low detectability. However, the samples may be damaged when using the method. The impurities found in the crystalline silicones used in solar panels are carbon impurities. Detecting impurity elements is difficult because carbon and silicon are congeners: substances with similar properties that prevent division. Binetti [13] studied the defects and impurities of multi-crystalline silicon grown from a metallurgical silicon feedstock. Rajasekhara [14] studied the effects of impurities and planar defects on the infrared properties of silicon carbide films. The present study proposed a lossless method for detecting carbon impurities in crystalline silicon in a geomagnetic field. This detection mechanism was proven via a magnetization test, theoretical analysis, and imaging technology. Metallographic phase and spectrum analysis verify that this method is effective in detecting carbon impurities in crystalline silicon.

2. Material and methods

2.1. Magnetization test and micromagnetic detection mechanism

A $200 \times 150 \times 150\ mm^3$ polysilicon bar was selected as the detected object. The magnetic properties of the polysilicon bar

* Corresponding author. Tel.: +86 18970037988; fax: +86 07913953467.
E-mail address: yurunqiao@163.com (R. Yu).
[1] These authors contributed equally to this work.

0963-8695/$ - see front matter © 2013 Elsevier Ltd. All rights reserved.
http://dx.doi.org/10.1016/j.ndteint.2013.10.003

were analyzed first. The magnet-measuring instrument of a superconducting quantum interference device (SQUID) was used to test the magnetization curve of the selected material at room temperature. Increasing the magnetic field applied decreases the magnetic moment in a linear fashion. Magnetic susceptibilities less than zero were solved through theoretical calculation [15]. Thus, the relative magnetic permeability of the silicon material ranged from 0.9999985 to 0.9999995. Therefore, the detected material was diamagnetic. The relative permeability of carbon is 0.999982, which is slightly less than that of the silicon material.

The diamagnetic features of the material showed that the magnetic induction intensity of the diamagnetic materials decreased with increasing applied magnetic field. When the strength of the applied magnetic field remained constant, the magnetic induction intensity decreased with increasing relative permeability. For the paramagnetic materials, magnetic induction intensity increased with increasing relative permeability.

Placing a tested sample with a relative permeability of μ in the geomagnetic field, the geomagnetic field can be seen as the applied magnetic field if there is a defect in the sample, and its relative permeability is μ'. Following the effect of the geomagnetic field on diamagnetic materials, the defect rejects the lines of the magnetic force when $\mu' > \mu$, making the lines more intense, where the two ends of the defect meet near the boundary of the sample. The magnetic induction intensity on the sample surface was more intense when no defects exist. Thus, an abnormal upward protuberance occurs. The defect draws the lines of the magnetic force closer when $\mu' < \mu$, making the lines loose where the two ends of the defect meet near the boundary of the sample. The magnetic induction intensity on the surface of the sample becomes looser when no defects exist. In this case, an abnormal downward protuberance occurs. Defects can be detected based on the abnormally-changed upward or downward projection by testing the changes in magnetic induction intensity using high-precision magnetic sensors.

2.2. Micromagnetic decay theory and calculation of apparent magnetic susceptibility parameter

Magnetic susceptibility is a physical quantity that represents the properties of a magnetic media, and can be regarded as the coefficient of material field attenuation penetrating through certain materials. The relative permeability is equal to susceptibility plus one. An apparent magnetic susceptibility parameter was defined here. The apparent magnetic susceptibility parameter can be calculated based on changes in the geomagnetic field intensity of the sample and the image was produced through changes in the apparent magnetic susceptibility parameter.

Micromagnetic decay theory is gained according to the energy decay. In the energy attenuation formula $I = I_0 e^{-\alpha T}$, I_0 is the strength of the applied energy, I is the magnitude of the applied energy going through the tested sample, α is the attenuation coefficient of the material, and T is the thickness of the tested sample. Thus, the strength attenuation formula of the magnetic field in the geomagnetic field can be deduced as $H \propto H_0 e^{-\chi T}$, where H_0 is the strength of the geomagnetic field and H is the strength of the geomagnetic field going through the tested sample. Given that $B = \mu_r H$, where μ_r is the relative permeability, then $B \propto B_0 e^{-\chi T}$, where B_0 is the magnetic induction intensity of the geomagnetic field and B is the magnetic induction intensity of the geomagnetic field going through the tested sample. If the scale coefficient was set as K, then $B \propto B_0 e^{-\chi T}$ can be expressed as $B = K B_0 e^{-\chi T}$. If K is used as an index and expressed by the constant K_1, then $B = B_0 e^{-K_1 \chi T}$, where $K_1\chi$ is the attenuation coefficient of the tested sample, which can be regarded as apparent magnetic susceptibility. The function e^x (set x as the independent variable), when expanded according to the power series formula, shows that when $|x| \ll 1$, and $e^x \approx 1 + x$. Therefore, when $|-K_1\chi T| \ll 1$, $e^{-K_1\chi T} \approx 1 - K_1\chi T$. The apparent magnetic susceptibility parameter can therefore be calculated using the following formula:

$$K_1\chi \approx (B_0 - B)/B_0 T \tag{1}$$

2.3. Imaging principle

The defect should not only be determined, but visualized via micromagnetic detection as well. The detection process was conducted using an array-type sensor composed of m-sensors that detect n points. Each detected points has a corresponding value of apparent magnetic susceptibility. Thus, the susceptibility of every group of data can be expressed by the array $m \times n$. Linear interpolation was used to remove the influence of inter-spaces between sensors. After linear interpolation, the array form of apparent magnetic susceptibility χ_r changes into the following:

$$\chi_r = \begin{pmatrix} \chi_{r11} & \cdots & \chi_{r1n} \\ \vdots & \ddots & \vdots \\ \chi_{rm1} & \cdots & \chi_{rmn} \end{pmatrix} \tag{2}$$

Every element in the function array matches a specific value of apparent magnetic susceptibility. The image of the defects can be expressed using the function array. In this manner, 2D imaging of the defects can be achieved.

The tested cubic silicon bar is shown in Fig. 1(a). The direction of the arrow indicates the direction of the probe on the surface. Data collected from side A denotes the strength of the geomagnetic field on the *XY* surface after going through the tested bar; the locations of the abnormal points on the A side in the direction of the *Z*-axis are unknown. Similarly, only the magnetic field strength of the bar on the surface of *YZ* can be found on the B side; the locations of the abnormal points on the B side in the direction of the *X*-axis are unknown. The specific coordinates of abnormal points (x, y, z) in the detected bar can be deduced based on the

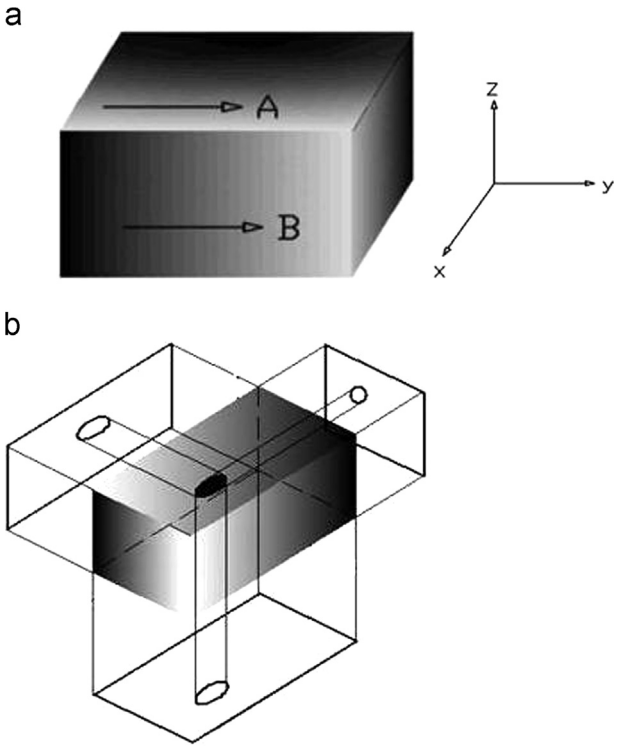

Fig. 1. The detected bar image (a) and diagram of the projection (b).